

Axonal and myelin changes and their inter-relationship in the optic radiations in people with multiple sclerosis

Eva A. Krijnen , Chanon Ngamsombat, Ilena C. George, Fang F. Yu, Qiuyun Fan, Qiyuan Tian, Susie Y. Huang  and Eric C. Klawiter

Multiple Sclerosis Journal—
Experimental, Translational
and Clinical

January–March 2023, 1–11

DOI: 10.1177/
20552173221147620

© The Author(s), 2023.
Article reuse guidelines:
sagepub.com/journals-
permissions

Abstract

Background: The imaging g-ratio, estimated from axonal volume fraction (AVF) and myelin volume fraction (MVF), is a novel biomarker of microstructural tissue integrity in multiple sclerosis (MS).

Objective: To assess axonal and myelin changes and their inter-relationship as measured by g-ratio in the optic radiations (OR) in people with MS (pwMS) with and without previous optic neuritis (ON) compared to healthy controls (HC).

Methods: Thirty pwMS and 17 HCs were scanned on a 3Tesla Connectom scanner. AVF and MVF, derived from a multi-shell diffusion protocol and macromolecular tissue volume, respectively, were measured in normal-appearing white matter (NAWM) and lesions within the OR and used to calculate imaging g-ratio.

Results: OR AVF and MVF were decreased in pwMS compared to HC, and in OR lesions compared to NAWM, whereas the g-ratio was not different. Compared to pwMS with previous ON, AVF and g-ratio tended to be higher in pwMS without prior ON. AVF and MVF, particularly in NAWM, were positively correlated with retinal thickness, which was more pronounced in pwMS with prior ON.

Conclusion: Axonal measures reflect microstructural tissue damage in the OR, particularly in the setting of remote ON, and correlate with established metrics of visual health in MS.

Keywords: Optic neuritis, multiple sclerosis, diffusion magnetic resonance imaging, optical coherence tomography, diffusion tractography, white matter

Background

The imaging g-ratio, defined as the ratio of inner axonal diameter to the diameter of axon plus myelin sheath, is an emerging biomarker of white matter (WM) microstructure and is calculated using estimates of axonal volume fraction (AVF) from diffusion-weighted magnetic resonance imaging (DW-MRI) and myelin volume fraction (MVF) from myelin-sensitive MRI methods.¹ Previous work on the imaging g-ratio in multiple sclerosis (MS) has demonstrated an increase in g-ratio in lesions compared to normal-appearing WM (NAWM), whereas both AVF and MVF were decreased in lesions compared to NAWM.^{2,3} The combination of myelin and axonal measures is thought to characterize tissue microstructure integrity more comprehensively than either measure in isolation, providing greater insight into

the relationship between demyelination and axonal loss.^{2,3}

Demyelination is the hallmark of MS pathology and frequently affects the visual pathway. Visual outcomes have been shown to be an accessible measure of disease activity and provide key insights into the pathophysiology of MS.^{4,5} Optic neuritis (ON) is the initial presentation in approximately 20% of people with MS (pwMS) and may occur in 50% of pwMS during the course of the disease.⁶ Retinal thinning, known to be a long-term consequence of ON, appears to be present in non-ON eyes as well to a lesser extent.^{7,8} Retinal thinning has been shown to be related to microstructural alterations in the optic radiations (OR) using diffusion tensor imaging and advanced diffusion models such as diffusion kurtosis

Correspondence to:
Eric C. Klawiter,
Department of Neurology,
Massachusetts General
Hospital, 15 Parkman Street,
Boston, MA 02114, USA.
eklawiter@mgh.harvard.edu

Eva A. Krijnen,
MS Center Amsterdam,
Anatomy and Neurosciences,
Amsterdam Neuroscience,
Amsterdam UMC location
VUmc, Amsterdam, The
Netherlands
Department of Neurology,
Massachusetts General
Hospital, Harvard Medical
School, Boston, MA, USA

Chanon Ngamsombat,
Department of Radiology,
Massachusetts General
Hospital, Harvard Medical
School, Athinoula



A. Martinos Center for Biomedical Imaging, Charlestown, MA, USA
Department of Radiology, Faculty of Medicine, Siriraj Hospital, Mahidol University, Bangkok, Thailand

Ilena C. George,
Department of Neurology, Massachusetts General Hospital, Harvard Medical School, Boston, MA, USA

Fang F. Yu,
Department of Radiology, University of Texas Southwestern Medical Center, Dallas, TX, USA

Qiyun Fan,
Department of Biomedical Engineering, College of Precision Instruments and Optoelectronics Engineering, Tianjin University, Tianjin, China
Academy of Medical Engineering and Translational Medicine, Medical College, Tianjin University, Tianjin, China

Qiyuan Tian,
Susie Y. Huang,
Department of Radiology, Massachusetts General Hospital, Harvard Medical School, Athinoula A. Martinos Center for Biomedical Imaging, Charlestown, MA, USA

Eric C. Klawiter,
Department of Neurology, Massachusetts General Hospital, Harvard Medical School, Boston, MA, USA

imaging and neurite orientation dispersion and density imaging.^{9–11} These prior studies primarily focused on analyses that consider axons as sticks, that is, with no measurable diffusivity within axons. Recent advances in gradient hardware for human MRI scanners have enabled high-sensitivity imaging of intra-axonal water diffusion, with the potential for greater sensitivity to axonal damage that is postulated to be a key substrate of neurodegeneration in MS.^{12–14}

The goal of this study was to assess axonal and myelin changes and their inter-relationship as measured by the *g*-ratio in the OR of pwMS with and without previous ON compared to healthy controls (HC) as measured on a dedicated high-gradient 3T MRI scanner. We sought to investigate the association between these axonal and myelin metrics and optical coherence tomography (OCT)-derived measurements of retinal thinning. We used an advanced multi-compartment model of intra-axonal water diffusion to evaluate microstructural changes in the OR between pwMS and HC and the effects of ON on OR axonal density and myelin volume in pwMS. We hypothesized that the *g*-ratio and its components are sensitive to myelin and axonal alterations in the OR as measured by high-gradient MRI and that these changes may reflect retinal thinning, independent of the history of ON, and visual dysfunction in pwMS.

Methods

Participants

This cross-sectional study was approved by the institutional review board and represents a targeted reanalysis of previously published data.² All participants provided written informed consent. Thirty participants with clinically diagnosed MS who visited the Massachusetts General Hospital MS Clinic between 2015 and 2019 were recruited as a convenience sample representative of MS and included a subset who had a prior history of ON. In addition, 17 HC were recruited for comparison. Of 30 pwMS, 24 participants had relapsing–remitting MS and six participants had progressive MS, including two participants with primary progressive MS and four participants with secondary progressive MS. Inclusion criteria for pwMS were a diagnosis of clinically definite MS, being relapse-free for >3 months, and, if treated, stable disease-modifying treatment for >6 months. Exclusion criteria were the presence of other structural brain diseases and contraindications to MRI. To assess neurological disability in

pwMS, an expanded disability status scale (EDSS) was used by a board-certified neurologist blinded to the imaging results. History of ON was clinically defined as an episode of sudden onset visual problems, including unilateral vision loss lasting for >24 h.

Image acquisition

MRI data were acquired prospectively using a dedicated high-gradient 3T MRI scanner (MAGNETOM Connectom; Siemens, Erlangen, Germany) equipped with maximum gradient strengths of 300 mT/m.^{12–14} A custom-built 64-channel phased array head coil was used for signal reception.¹⁵ DW-MRI data were acquired using a diffusion-weighted spin-echo single-shot echo planar imaging sequence in the sagittal plane ($2 \times 2 \times 2$ mm³ voxel size, echo time (TE)/repetition time (TR) = 77/3600 ms, simultaneous multi-slice imaging with slice acceleration factor 2, parallel imaging acceleration factor $R = 2$, and anterior-to-posterior phase encoding).¹⁶ Diffusion gradients were applied in 32 directions for *b*-values <2300 s/mm² and 64 directions for *b*-values >2300 s/mm², evenly distributed on a unit sphere. The maximum *b*-value was 17,800 s/mm². Five *b* = 0 images with the reversed-phase encoding direction were acquired for distortion correction. The DW-MRI protocol was designed to obtain reproducible estimates of apparent axon diameter and density within an hour of scan time (total acquisition time of 51 min).¹⁷

A multiple flip angle spoiled gradient-echo three-dimensional fast low-angle shot (3D-FLASH) sequence was used to acquire macromolecular tissue volume (MTV) data for myelin quantification (1 mm isotropic resolution, TE/TR = 2.74/20 ms, flip angle = 4°–10°–20°, 15 min total acquisition time (5 min per sequence)).¹⁸ Structural images were acquired including a T1-weighted multi-echo magnetization prepared rapid gradient echo imaging (MPRAGE) sequence (1 mm isotropic resolution, TE/TR/inversion time (TI) = 1.15–3.03–4.89–6.75 ms/2530 ms/1100 ms, $R = 3$, flip angle = 7°, 3 min 58 s acquisition time), and three-dimensional fluid-attenuated inversion recovery (3D-FLAIR) sequence (0.9 mm isotropic resolution, TE/TR/TI = 389 ms/5000 ms/1800 ms, $R = 2$, 5 min 47 s acquisition time).

Data processing

Diffusion MRI data. All images were corrected for gradient nonlinearity using in-house software.¹⁹ Image distortions due to susceptibility and eddy

current effects were corrected using “topup” and “eddy” in FSL (<https://fsl.fmrib.ox.ac.uk>).^{20,21}

A previously published method for extracting measures of axonal diameter and density independent of fiber orientation was used to estimate cerebrospinal fluid (CSF) and restricted water volume fractions.²² A three-compartment model was used to represent the restricted diffusion within impermeable cylindrical axons of finite diameter, hindered Gaussian diffusion in the extra-axonal space, and free diffusion in CSF. The longitudinal diffusivity was assumed to be the same for intracellular and extracellular compartments and was fixed at $1.7 \times 10^{-3} \text{ mm}^2/\text{s}$. The free diffusion coefficient was assumed to be equal to free water diffusivity at 37°C ($3 \times 10^{-3} \text{ mm}^2/\text{s}$). Markov Chain Monte-Carlo sampling was used to fit the spherically averaged form of the signal model, yielding orientation-independent estimates of axon diameter index, perpendicular diffusivity of the hindered water compartment, and volume fractions of restricted water and CSF compartments.²² Restricted water and CSF volume fractions were used in the g-ratio calculation.

Macromolecular tissue volume. MTV has been demonstrated to be sensitive to myelin primarily based on the relationship with other quantitative myelin mapping techniques in the MS brain.²³ 3D-FLASH images were corrected for B_1 inhomogeneity using actual flip angle imaging.²⁴ FSL Linear Registration Tool was used to co-register the images acquired at the three flip angles (<http://www.fmrib.ox.ac.uk/fsl/fslwiki/FLIRT>). Equilibrium magnetization M_0 and T1 values were estimated on a voxel-wise basis.²³ MTV was computed as¹⁸

$$\text{MTV} = 1 - \frac{\text{Proton density}}{\text{Proton density of free water}}$$

Registration and segmentation

Regions of interest (ROIs) within the lateral geniculate nucleus (LGN) and WM of the primary visual cortex of the occipital lobe were generated as follows. The LGN ROI was derived using a probabilistic atlas of human thalamic nuclei in FreeSurfer,²⁵ converted into binary masks, and transformed to DW-MRI space using the FreeSurfer boundary-based registration tool.²⁶ For each hemisphere, the primary visual cortex target ROI was derived from FreeSurfer.²⁷ To capture as many fibers as possible originating from the LGN and extending to the cortex, a 1 mm ribbon of subcortical WM deep to

the gray–white junction was sampled from the primary visual cortex ROI.⁹

Lesion segmentation was performed on the 3D-FLAIR images of all pwMS. First, the boundary-based registration tool²⁶ was used to register FLAIR images to T1-weighted images. Automatic segmentation of FLAIR hyperintense lesions was performed using a FreeSurfer-based validated tool.²⁸ Lesion masks were manually edited by two board- and subspecialty-certified neuroradiologists. To generate NAWM masks, lesion masks were subtracted from the OR masks, yielding three masks per subject: lesion mask, NAWM mask, and an entire OR mask including both lesions and NAWM. Lesion volume was measured in both OR and averaged for subsequent analysis.

Diffusion tractography

Distributions of voxel-wise crossing fiber orientation were generated for probabilistic tractography using the FSL “bedpostx” function. The multi-shell option with $b = 800, 1500, \text{ and } 2400 \text{ s/mm}^2$ data was used for “bedpostx” fitting, assuming a “ball and two-stick” model and Rician noise. Probabilistic tractography was performed using the FSL “probtrackx2” function²⁹ in two directions (LGN to ipsilateral primary visual cortex, and vice versa). A corpus callosum mask served as an exclusion mask. From each voxel, 5000 streamlines were generated in the seed ROI, and only those passing through the ipsilateral target ROI, and not entering the exclusion mask, were retained. A 1% tract threshold was set to binarize the probabilistic tractography results, tracking from LGN to the ipsilateral primary visual cortex and primary visual cortex to LGN with the inclusion of Meyer’s loop as part of the OR, yielding a binarized mask of the bilateral OR (Figure 1).

G-ratio calculation

The CSF and restricted water volume fractions as well as MVF (based on MTV) were used to calculate the g-ratio.²³ The AVF was calculated by combining MTV, CSF, and restricted volume fractions^{1,23}:

$$\text{AVF} = (1 - \text{MTV}) \times (1 - \text{CSF volume fraction}) \\ \times \text{restricted volume fraction}$$

The g-ratio was computed as¹

$$g\text{-ratio} = \sqrt{\frac{1}{1 + (\text{MTV}/\text{AVF})}}$$

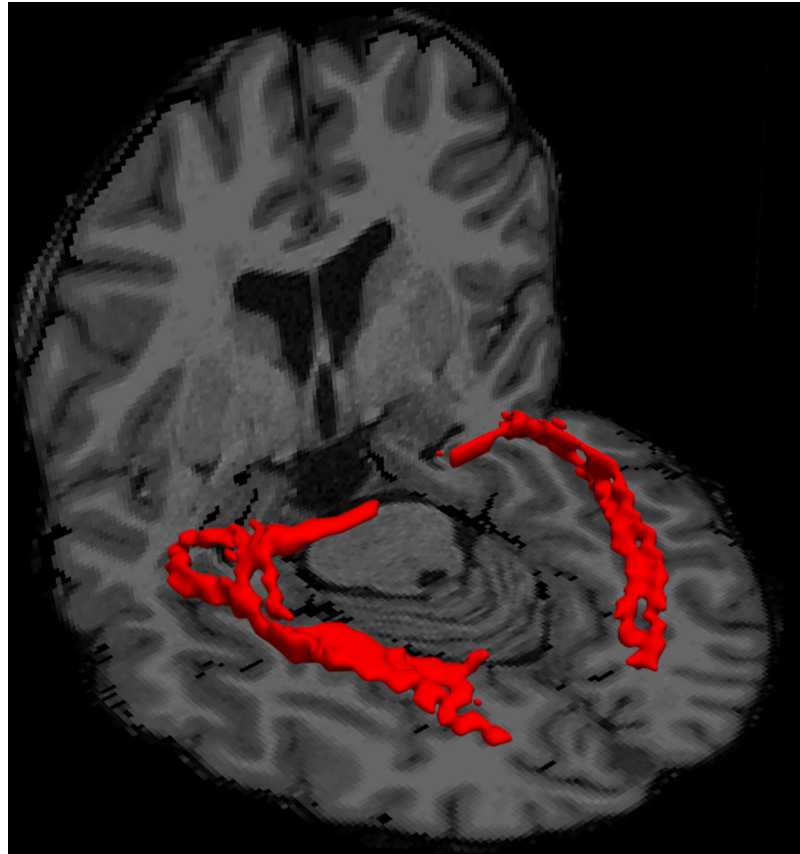


Figure 1. Volume rendered results of the thresholded tractography results of the optic radiation in a representative multiple sclerosis (MS) patient (red).

Entire OR, lesion, and NAWM masks were overlaid on the whole-brain g-ratio, and AVF and MVF maps were used to generate three separate masks per magnetic resonance (MR) metric.

Optical coherence tomography

OCT data were acquired and retrospectively reported in accordance with the updated APOSTEL 2.0 guidelines,³⁰ with further clarification upon reasonable request. For each MS patient, spectral domain OCT was conducted <30 days of the MRI using a Zeiss Cirrus HD-OCT instrument at one operating site by an experienced technician (model 4000-4648, software version 7.0.3.19). Scans acquired in both non-dilated eyes were Macular Cube Scan 512×128 and Optic Disc Cube 200×200. Requirements were scanning in a dark room and a minimum signal strength of 7. OSCAR-IB [(O)=obvious problems including violation of the protocol; (S) poor signal strength defined as <15 dB; (C) wrong centration of scan; (A) algorithm failure; (R) retinal pathology other than MS related; (I) illumination; and (B) beam placement] quality control criteria were used to ensure the quality of our

OCT scans with at least 5 of 7 criteria fulfilled in all participants.³¹ Retinal nerve fiber layer (RNFL) and the ganglion cell layer combined with the inner plexiform layer (GCIPL) were automatically segmented by the scanner in all four quadrants (nasal, superior, temporal, inferior) and averaged. RNFL and GCIPL thickness of the non-affected eye (eye without prior ON) were used in correlation analysis. Of participants without prior ON, OCT measures were averaged across both eyes. Participants with a history of bilateral ON were excluded from OCT analyses.

Visual acuity

Visual acuity (VA) was measured in pwMS using both high (100%) and low-contrast (2.5% and 1.25%) letter acuity Sloan charts.³² VA was tested at a 2 m distance in a well-lit room. The number of correctly identified letters (maximum 60 letters per chart) was reported for each eye. VA was best corrected, and again measures of the non-affected eye were reported. For participants without prior ON, VA scores were averaged across both eyes. Based on prior work showing that severe optic nerve

damage might mask or interfere with the relationship between the OR and visual functioning,¹⁰ only participants with an average RNFL >80µm of non-affected eyes were included in the VA analysis.

Statistical analysis

Statistical analysis was performed in IBM SPSS Statistics for Macintosh (version 25.0; IBM Corp., Armonk, NY, USA). Shapiro-Wilk's test and histogram inspection were used to assess the normality of the data. To compare demographic, clinical, OCT, and MRI variables between pwMS and HC, student's *t*-tests and chi-square tests were used for continuous variables and nominal variables, respectively. The same tests were used to compare pwMS with and without prior ON. Within-subject differences in AVF, MVF, and g-ratio between NAWM and lesions in pwMS were assessed with paired *t*-tests. Pearson's correlation coefficient was used to test for relationships between entire OR measures and OCT and VA data; if significant, results were further analyzed specifically in NAWM and lesional OR. Corrections for multiple comparisons were conducted based on Bonferroni correction with $\alpha = 0.05$.

Results

Patient characteristics

Table 1 shows the demographics and MR metrics of all participants. Demographics and clinical characteristics did not significantly differ between groups. The mean disease duration of pwMS was 9.55 years. Median EDSS was 2.0, corresponding to mild disease severity. Whole-brain lesion volume as well as OR lesion volume varied across pwMS (means of 7,166 mm³, range 174–48,043 mm³, and 185 mm³, range 0–2083 mm³, respectively). Eighteen pwMS (60%) had a history of ON, of whom seven (23.3%) had ON in each eye at some point in their course, typically sequentially, and were excluded from the correlation analysis of MRI and OCT outcomes.

OR measures

Figure 2 shows the variation in AVF, MVF, and g-ratio in NAWM and lesional OR. AVF and MVF in NAWM OR were decreased in pwMS compared to HC (0.227 vs. 0.260, $p < 0.001$; 0.268 vs. 0.290, $p = 0.045$) (Figure 3). After Bonferroni correction, only differences in OR AVF remained significant. G-ratio did not differ between pwMS and HC. In pwMS, OR AVF and MVF were significantly lower in lesions compared to NAWM (0.158 vs. 0.231, $p < 0.001$; 0.200 vs. 0.265, $p < 0.001$). The OR g-ratio did not differ between lesions and NAWM (Figure 4).

History of ON

Compared to pwMS with previous ON, AVF and g-ratio in the entire OR (including NAWM and lesions) were higher in pwMS without prior ON ($p = 0.01$ and $p = 0.04$, respectively) (Table 2). AVF and g-ratio in the OR NAWM were higher in pwMS without prior ON compared to pwMS with prior ON ($p = 0.03$ and $p = 0.05$, respectively). However, after Bonferroni correction, no differences remained significant in either the entire OR or the segmented NAWM.

Optic coherence tomography

OR AVF showed positive correlations with RNFL and GCIPL ($r = 0.63$, $p = 0.001$ and $r = 0.66$, $p = 0.001$, respectively) (Table 3). Subanalysis showed moderate positive correlations between AVF in NAWM and lesions and RNFL and GCIPL (r -range = 0.51–0.54, p -range = 0.008–0.02). OR MVF was significantly correlated with GCIPL ($r = 0.58$, $p = 0.004$); however, MVF specifically in NAWM and in lesions did not show any significant correlations with OCT data.

Focusing the analysis on pwMS with previous ON, RNFL had a strong correlation with OR AVF ($r = 0.81$, $p = 0.003$), particularly in NAWM ($r = 0.75$, $p = 0.008$). Also, GCIPL showed a strong positive correlation with OR AVF ($r = 0.76$, $p = 0.007$). In addition, a strong correlation was present between GCIPL and OR MVF ($r = 0.75$, $p = 0.007$), again particularly in NAWM ($r = 0.71$, $p = 0.02$). In pwMS without previous ON, RNFL thinning was moderately associated with reduced OR g-ratio and AVF ($r = 0.63$, $p = 0.03$ and $r = 0.59$, $p = 0.04$, respectively); however, no correlations survived Bonferroni correction (Supplementary Table 1).

Visual acuity

Five pwMS had an average RNFL <80 µm, so were excluded from the VA analysis. OR g-ratio and AVF showed moderate negative correlations with low-contrast (1.25%) VA ($r = -0.61$, $p = 0.007$, and $r = -0.51$, $p = 0.03$, respectively) (Supplementary Table 2). After the Bonferroni correction, there were no significant correlations between VA scores and MRI metrics, so the results were not analyzed further.

Discussion

In this study, we evaluated changes in axonal and myelin measures obtained from high-gradient MRI and their inter-relationship as measured by g-ratio in the OR of pwMS with and without previous ON and investigated the association between these

Table 1. Demographics of HC and pwMS both with and without history of ON.

	HC	pwMS	<i>p</i>	pwMS with prior ON	pwMS without prior ON	<i>p</i>
<i>N</i>	17 (36.2)	30 (63.8)		18 (60.0)	12 (40.0)	
Age	42.5 (14.2)	42.9 (11.7)	ns	41.6 (13.1)	44.8 (9.6)	ns
Sex, female	10 (58.8)	23 (76.7)	ns	15 (83.3)	8 (66.7)	ns
Disease duration in years	—	9.2 (6.66)	—	9.6 (7.3)	8.7 (5.8)	ns
MS subtype						
Relapsing–remitting	—	24 (80.6)	—	13 (72.2)	11 (91.7)	
Primary progressive	—	2 (6.5)	—	1 (5.6)	1 (8.3)	ns
Secondary progressive	—	4 (12.9)	—	4 (22.2)	0 (0)	
Use of disease-modifying therapy ^a	—	27 (90.0)	—	16 (88.9)	11 (91.7)	ns
Expanded disability status scale	—	2.0 [1.38–3.13]	—	2.3 [1.0–3.63]	2.0 [2.0–3.0]	ns
Lesion volume in mL	—	7.2 (10.4)	—	9.7 (12.9)	3.4 (2.2)	ns
OR lesion volume in mL	—	0.19 (0.42)	—	0.29 (0.53)	0.033 (0.038)	ns
History of ON						
Left	—	6 (20.0)	—	6 (20.0)	—	—
Right	—	5 (16.7)	—	5 (16.7)	—	—
Bilateral	—	7 (23.3)	—	7 (23.3)	—	—
Duration since ON in years ^b	—	7.9 (7.4)	—	7.9 (7.4)	—	—
RNFL in μm						
Non-affected eyes	—	93.0 (16.0)	—	92.6 (17.3)	93.3 (15.5)	ns
Affected eyes	—	81.1 (14.9)	—	81.1 (14.9)	—	—
GCIPL in μm						
Non-affected eyes	—	78.8 (11.4)	—	76.5 (14.4)	80.9 (7.8)	ns
Affected eyes	—	69.5 (13.2)	—	69.5 (13.2)	—	—
VA 100% in %-correct						
Non-affected eyes	—	50.0 (10.0)	—	48.5 (13.7)	51.4 (5.1)	ns
Affected eyes	—	45.9 (15.5)	—	45.9 (15.5)	—	—
VA 2.5% in %-correct						
Non-affected eyes	—	25.6 (11.5)	—	26.9 (12.7)	24.5 (10.8)	ns
Affected eyes	—	17.1 (11.2)	—	17.1 (11.2)	—	—
VA 1.25% in %-correct						
Non-affected eyes	—	8.4 (8.9)	—	12.7 (10.3)	4.5 (5.2)	0.03
Affected eyes	—	4.6 (7.2)	—	4.6 (7.2)	—	—

HC: healthy controls; MS: multiple sclerosis; pwMS: people with MS; OR: optic radiations; ON: optic neuritis; RNFL: retinal nerve fiber layer; GCIPL: ganglion cell layer plus inner plexiform layer; VA: visual acuity; ns: not significant; SD: standard deviation.

Demographics and MR measures were reported as number (%), mean (SD), or median (interquartile range).

^a9 pwMS were taking dimethyl fumarate, 5 glatiramer acetate, 3 fingolimod, 4 interferon beta (1a/1b), 2 ocrelizumab, 2 natalizumab, 2 rituximab.

^bIn the case of bilateral optic neuritis, the first episode is included.

metrics and both RNFL and GCIPL thinning as measured by OCT. Our results show that AVF in particular can detect differences in the OR between pwMS and HC and between NAWM and demyelinating lesions, whereas the g-ratio did not differ.

Participants with prior ON showed trends toward lower OR AVF and g-ratio values compared to participants without prior ON, whose AVF and g-ratio were closer to HC. These differences were more prominent in NAWM than in lesions. Moreover,

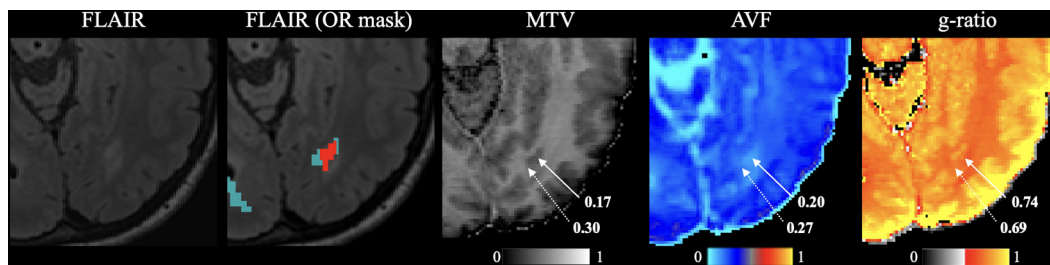


Figure 2. Representation of NAWM (light blue; second image) and lesional (red; second image) OR on axial FLAIR image and maps of corresponding MVF (third image), AVF (fourth image), and g-ratio (fifth image). Solid arrows indicate lesions. Dotted arrows indicate NAWM.

NAWM: normal-appearing white matter; OR: optic radiations; FLAIR: fluid-attenuated inversion recovery; MVF: myelin volume fractions; AVF: axonal volume fraction.

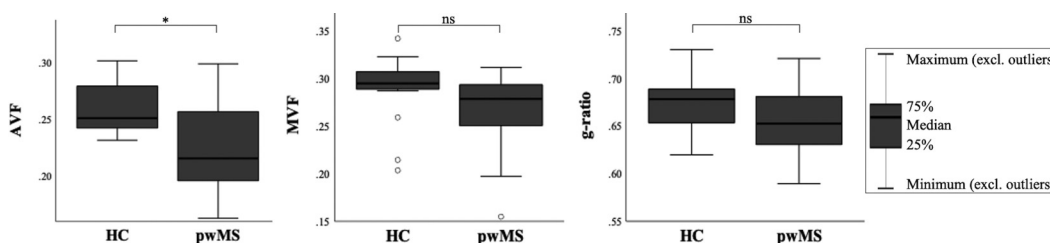


Figure 3. Differences in MR metrics in the optic radiations between pwMS and HC. AVF, MVF, and g-ratio are reported as median values with interquartile range and minimum and maximum values for both pwMS and HC. Open circles in the MVF plot denote outliers. Differences between pwMS and HC surviving Bonferroni correction are marked with an asterisk (*); others are denoted as ns.

pwMS: people with multiple sclerosis; HC: healthy controls; AVF: axonal volume fraction; MVF: myelin volume fraction; ns: not significant.

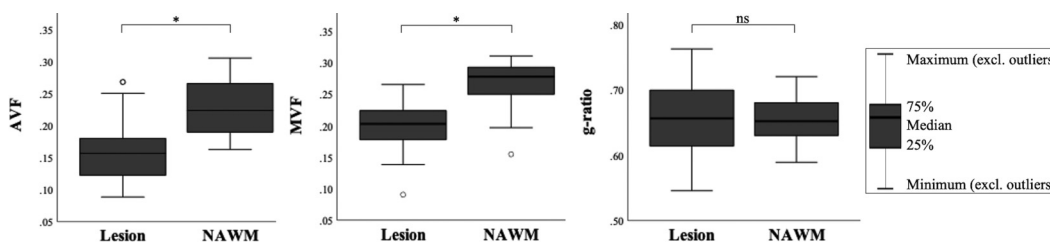


Figure 4. Differences in MR metrics in the optic radiations between lesions and NAWM. AVF, MVF, and g-ratio are reported as median values with interquartile range and minimum and maximum values for both NAWM and lesions. Open circles in the AVF and MVF plots denote outliers. Differences between NAWM and lesions surviving Bonferroni correction are marked with an asterisk (*); others are denoted as ns.

NAWM: normal-appearing white matter; AVF: axonal volume fraction; MVF: myelin volume fractions; ns: not significant.

participants with previous ON showed stronger correlations between AVF and MVF and retinal thickness than participants without a history of ON. We postulate that ON may affect axonal density, leading to neurodegeneration in the OR. Alternatively, axonal degeneration in the OR has also been postulated to lead to retinal thinning in pwMS.³³

Besides focal lesions, there is a more widespread, diffuse neurodegeneration in the NAWM of pwMS,³⁴ which is supported by our finding that in particular, AVF in the OR NAWM was lower in pwMS than HC. Prior work of our group more generally demonstrated an increase in WM g-ratio in pwMS compared to HC and more so within lesions.² These differences were less apparent when focusing our

Table 2. MR metrics in the OR of people with MS with and without prior ON.

	Participants with prior ON (N = 18)			Participants without prior ON (N = 12)			p-value
	Entire OR	NAWM	Lesion	Entire OR	NAWM	Lesion	
AVF	0.2076 (0.0403)	0.2124 (0.0348)	0.1549 (0.0498)	0.2510 (0.0461)	0.2480 (0.0472)	0.1624 (0.0456)	0.01
MVF	0.2631 (0.0435)	0.2674 (0.0369)	0.2011 (0.0435)	0.2708 (0.0313)	0.2693 (0.0355)	0.1978 (0.0397)	0.60
G-ratio	0.6470 (0.0329)	0.6472 (0.0302)	0.6519 (0.0633)	0.6756 (0.0385)	0.6721 (0.0358)	0.6630 (0.0614)	0.04

MR: magnetic resonance; MS: multiple sclerosis; ON: optic neuritis; NAWM: normal-appearing white matter; AVF: axonal volume fraction; MVF: myelin volume fraction; OR: optic radiations; SD: standard deviation;
 AVF, MVF, and g-ratio of the entire OR, NAWM, and lesions were reported as means with SD. Raw unadjusted p-values were reported here. No p-values survived Bonferroni correction.

Table 3. Relationship between optical coherence tomography measures and MR metrics in the OR.

	AVF			MVF			G-ratio		
	Entire OR	NAWM	Lesion	Entire OR	NAWM	Lesion	Entire OR	NAWM	Lesion
RNFL	0.632 (0.001*)	0.531 (0.009*)	0.514 (0.02)	0.428 (0.04)	—	—	0.382 (0.07)	—	—
GCIPL	0.657 (0.001*)	0.537 (0.008*)	0.455 (0.04)	0.582 (0.004*)	0.444 (0.03)	0.347 (0.13)	0.267 (0.22)	—	—

MR: magnetic resonance; OR: optic radiations; AVF: axonal volume fraction; MVF: myelin volume fraction; NAWM: normal-appearing white matter; RNFL: retinal nerve fiber layer; GCIPL: ganglion cell layer plus inner plexiform layer.
 Pearson's correlation coefficients with raw unadjusted p-values were reported for AVF, MVF, and g-ratio correlations. Dash (—) denotes subanalysis was not performed because of the non-significance of the main result. P-values surviving Bonferroni correction are marked with an asterisk (*).

analysis on the OR, perhaps due to the effect of prior disease in the optic nerve that would be expected to produce a more proportional effect on myelin and axons in the OR, yielding a similar g-ratio. In addition, both AVF and MVF were significantly lower in OR lesions compared to NAWM, as supported by prior studies investigating axonal and myelin loss in MS.^{1,2} Chronic lesions would be expected to demonstrate g-ratio values closer to NAWM as they are characterized by demyelination and axonal degeneration rather than primarily demyelination seen in acute lesions.^{34,35} While the relevance of the imaging g-ratio may appear limited in the OR, we are restricted from drawing these conclusions due to the cross-sectional design of this study. Our findings emphasize the importance of studying relative changes in AVF and MVF over time to further tease out the pathophysiological mechanisms driving the degree of demyelination and axonal loss in the MS brain and to consider those changes together.

Local, acute neuronal damage in inflammatory lesions in the OR is related to visual disability and retinal damage.^{36,37} The observed decrease in normal-appearing OR AVF and MVF of pwMS is significantly correlated with retinal damage as well, a finding that is in line with previous studies investigating the relationship between OCT and OR diffusion measures.^{9,10,38} Notably, the OR fractional anisotropy, which is thought to be provided by both the axon itself and its myelination, was decreased in pwMS and associated with retinal thinning.^{10,38} Also, a study investigating advanced diffusion metrics in the OR found that the axonal water fraction was associated with RNFL thickness in pwMS without a history of ON to the same extent as in our study ($r = 0.68$ vs. $r = 0.59$).⁹ Chronic demyelination of the optic nerve after an episode of ON is found to accelerate retinal damage in both affected and non-affected eyes.³⁹ As the relation found between retinal damage and OR metrics was more pronounced in the setting of remote ON, this provides further evidence linking prior disease in the optic nerve and clinical functioning in ON to accumulating axonal damage and demyelination of the OR in MS—two structures that are synaptically connected at the LGN. As this process might evolve slowly and its effects might be mild,³⁹ long-term monitoring is required to establish and reliably measure the neurodegenerative consequences of optic nerve demyelination.

A strength of our study was the use of advanced neuroimaging measures to estimate AVF, MVF, and g-ratio. In particular, the use of high-gradient diffusion

MRI may provide a higher signal-to-noise ratio and more robust estimates of CSF and restricted water fractions, increasing the sensitivity of probing smaller diameter axons. However, these methods require further validation on other 3T systems with conventional and high-gradient strengths, which are becoming increasingly prevalent as high-performance gradient technology improves.^{14,40,41} Additionally, we applied a relatively novel and accurate approach to reconstruct the OR fiber tracts. For fiber tracking, we used “probtrackx2” and selected our ROIs by a semi-automated segmentation of FreeSurfer, which has been shown to reconstruct fiber tracts accurately and reproducibly.⁴² As other studies applied different approaches for OR reconstruction, direct comparison is limited.

Our study is limited by the small sample size and heterogeneity of the cohort, restricting the statistical power of our analyses, which implies that significant results are relevant but provisional. As already pointed out, due to the cross-sectional study design, we were only able to investigate associations rather than causality between retinal thickness and OR measures. Larger longitudinal studies are needed to evaluate the possible causal relationship between those two.

In conclusion, AVF, MVF, and imaging g-ratio reflect microstructural tissue damage in the OR, particularly in the setting of remote ON, and correlate with established metrics of visual health. Axonal, and to a lesser extent myelin, changes are observed in the setting of remote ON, suggesting axonal measures play an important role in modulating clinical functioning after ON. Preservation of axons is therefore important as it relates to visual recovery. Further research should investigate the use of this method in measuring remyelination after an acute demyelinating event.

Declaration of conflicting interests



The author(s) declared the following potential conflicts of interest with respect to the research, authorship, and/or publication of this article: I.C.G. became employed by Biogen following her contributions to this research. S.Y.H. has received consulting fees and research grants from Siemens Healthineers. E.C.K. has received consulting fees from Banner Life Sciences, Galen/Atlantica, Genentech, Greenwich Biosciences and OM1, and research funds from Abbvie, Biogen, and Genentech. Other authors report no potential conflicts of interest with respect to the research, authorship, and/or publication of this article.

Funding

The author(s) disclosed receipt of the following financial support for the research, authorship, and/or publication of

this article: This work was supported by the National Institutes of Health (grant numbers K23-NS096056, P41-EB015896, P41-EB030006, R01-NS118187, and U01-EB026996)

ORCID iDs

Eva A. Krijnen  <https://orcid.org/0000-0002-3628-4127>
Susie Y. Huang  <https://orcid.org/0000-0003-2950-7254>

Supplemental material

Supplemental material for this article is available online.

References

1. Stikov N, Campbell JS, Stroh T, et al. In vivo histology of the myelin g-ratio with magnetic resonance imaging. Research support, non-U.S. Gov't. *NeuroImage* 2015; 118: 397–405.
2. Yu F, Fan Q, Tian Q, et al. Imaging G-ratio in multiple sclerosis using high-gradient diffusion MRI and macromolecular tissue volume. *AJNR Am J Neuroradiol* 2019; 40: 1871–1877.
3. Hagiwara A, Hori M, Yokoyama K, et al. Analysis of white matter damage in patients with multiple sclerosis via a novel in vivo MR method for measuring myelin, axons, and G-ratio. *AJNR Am J Neuroradiol* 2017; 38: 1934–1940.
4. Frohman EM, Frohman TC, Zee DS, et al. The neuro-ophthalmology of multiple sclerosis. *Lancet Neurol* 2005; 4: 111–121.
5. Graves JS, Oertel FC, Van der Walt A, et al. Leveraging visual outcome measures to advance therapy development in neuroimmunologic disorders. *Neurol Neuroimmunol Neuroinflamm* 2021; 9: e1126.
6. Arnold AC. Evolving management of optic neuritis and multiple sclerosis. *Am J Ophthalmol* 2005; 139: 1101–1108.
7. Denis M, Woillez JP, Smirnov VM, et al. Optic nerve lesion length at the acute phase of optic neuritis is predictive of retinal neuronal loss. *Neurol Neuroimmunol Neuroinflamm* 2022; 9: e1135.
8. Sepulcre J, Murie-Fernandez M, Salinas-Alaman A, et al. Diagnostic accuracy of retinal abnormalities in predicting disease activity in MS. *Neurology* 2007; 68: 1488–1494.
9. Ngamsombat C, Tian Q, Fan Q, et al. Axonal damage in the optic radiation assessed by white matter tract integrity metrics is associated with retinal thinning in multiple sclerosis. *NeuroImage Clin* 2020; 27: 102293.
10. Reich DS, Smith SA, Gordon-Lipkin EM, et al. Damage to the optic radiation in multiple sclerosis is associated with retinal injury and visual disability. *Arch Neurol* 2009; 66: 998–1006.
11. Manogaran P, Vavasour IM, Lange AP, et al. Quantifying visual pathway axonal and myelin loss in multiple sclerosis and neuromyelitis optica. *NeuroImage Clin* 2016; 11: 743–750.
12. Setsompop K, Kimmlingen R, Eberlein E, et al. Pushing the limits of in vivo diffusion MRI for the human connectome project. *NeuroImage* 2013; 80: 220–233.
13. McNab JA, Edlow BL, Witzel T, et al. The human connectome project and beyond: initial applications of 300 mT/m gradients. *NeuroImage* 2013; 80: 234–245.
14. Fan Q, Eichner C, Afzali M, et al. Mapping the human connectome using diffusion MRI at 300 mT/m gradient strength: methodological advances and scientific impact. *NeuroImage* 2022; 07: 118958.
15. Keil B, Blau JN, Biber S, et al. A 64-channel 3T array coil for accelerated brain MRI. *Magn Reson Med* 2013; 70: 248–258.
16. Huang SY, Tian Q, Fan Q, et al. High-gradient diffusion MRI reveals distinct estimates of axon diameter index within different white matter tracts in the in vivo human brain. *Brain Struct Funct* 2020; 225: 1277–1291.
17. Fan Q, Polackal MN, Tian Q, et al. Scan-rescan repeatability of axonal imaging metrics using high-gradient diffusion MRI and statistical implications for study design. *NeuroImage* 2021; 240: 118323.
18. Mezer A, Yeatman JD, Stikov N, et al. Quantifying the local tissue volume and composition in individual brains with magnetic resonance imaging. *Nat Med* 2013; 19: 1667–1672.
19. Fan Q, Witzel T, Nummenmaa A, et al. MGH-USC human connectome project datasets with ultra-high b-value diffusion MRI. *NeuroImage* 2016; 124: 1108–1114.
20. Andersson JLR and Sotiropoulos SN. An integrated approach to correction for off-resonance effects and subject movement in diffusion MR imaging. *NeuroImage* 2016; 125: 1063–1078.
21. Smith SM, Jenkinson M, Woolrich MW, et al. Advances in functional and structural MR image analysis and implementation as FSL. *NeuroImage* 2004; 23: S208–S219.
22. Fan Q, Nummenmaa A, Witzel T, et al. Axon diameter index estimation independent of fiber orientation distribution using high-gradient diffusion MRI. *NeuroImage* 2020; 222: 117197.
23. Duval T, Le Vy S, Stikov N, et al. g-Ratio weighted imaging of the human spinal cord in vivo. *NeuroImage* 2017; 145: 11–23.
24. Yarnykh VL. Actual flip-angle imaging in the pulsed steady state: a method for rapid three-dimensional mapping of the transmitted radiofrequency field. *Magn Reson Med* 2007; 57: 192–200.
25. Iglesias JE, Insausti R, Lerma-Usabiaga G, et al. A probabilistic atlas of the human thalamic nuclei combining ex vivo MRI and histology. *NeuroImage* 2018; 183: 314–326.
26. Greve DN and Fischl B. Accurate and robust brain image alignment using boundary-based registration. Evaluation studies research support, N.I.H., extramural research support, non-U.S. Gov't. *NeuroImage* 2009; 48: 63–72.
27. Fischl B, Rajendran N, Busa E, et al. Cortical folding patterns and predicting cytoarchitecture. *Cereb Cortex* 2008; 18: 1973–1980.

28. Lindemer ER, Salat DH, Smith EE, et al. White matter signal abnormality quality differentiates mild cognitive impairment that converts to Alzheimer's disease from nonconverters. *Neurobiol Aging* 2015; 36: 2447–2457.
29. Behrens TE, Berg HJ, Jbabdi S, et al. Probabilistic diffusion tractography with multiple fibre orientations: What can we gain? *NeuroImage* 2007; 34: 144–155.
30. Aytulun A, Cruz-Herranz A, Aktas O, et al. APOSTEL 2.0 recommendations for reporting quantitative optical coherence tomography studies. *Neurology* 2021; 97: 68–79.
31. Schippling S, Balk LJ, Costello F, et al. Quality control for retinal OCT in multiple sclerosis: validation of the OSCAR-IB criteria. *Mult Scler* 2015; 21: 163–170.
32. Balcer LJ, Raynowska J, Nolan R, et al. Validity of low-contrast letter acuity as a visual performance outcome measure for multiple sclerosis. *Mult Scler* 2017; 23: 734–747.
33. Balk LJ, Steenwijk MD, Tewarie P, et al. Bidirectional trans-synaptic axonal degeneration in the visual pathway in multiple sclerosis. *J Neurol Neurosurg Psychiatry* 2015; 86: 419–424.
34. Fitzner D and Simons M. Chronic progressive multiple sclerosis – pathogenesis of neurodegeneration and therapeutic strategies. *Curr Neuropharmacol* 2010; 8: 305–315.
35. Simkins TJ, Duncan GJ and Bourdette D. Chronic demyelination and axonal degeneration in multiple sclerosis: pathogenesis and therapeutic implications. *Curr Neurol Neurosci Rep* 2021; 21: 26.
36. Sinnecker T, Oberwahrenbrock T, Metz I, et al. Optic radiation damage in multiple sclerosis is associated with visual dysfunction and retinal thinning—an ultrahigh-field MR pilot study. *Eur Radiol* 2015; 25: 122–131.
37. Klistorner A, Graham EC, Yiannikas C, et al. Progression of retinal ganglion cell loss in multiple sclerosis is associated with new lesions in the optic radiations. *Eur J Neurol* 2017; 24: 1392–1398.
38. Klistorner A, Sriram P, Vootakuru N, et al. Axonal loss of retinal neurons in multiple sclerosis associated with optic radiation lesions. Research support non-U.S. gov't. *Neurology* 2014; 82: 2165–2172.
39. Klistorner A, Klistorner S, You Y, et al. Long-term effect of permanent demyelination on axonal survival in multiple sclerosis. *Neurol Neuroimmunol Neuroinflamm* 2022; 9: e1135.
40. Huang SY, Witzel T, Keil B, et al. Connectome 2.0: developing the next-generation ultra-high gradient strength human MRI scanner for bridging studies of the micro-, meso- and macro-connectome. *Neuroimage* 2021; 243: 118530.
41. Vachha B and Huang SY. MRI With ultrahigh field strength and high-performance gradients: challenges and opportunities for clinical neuroimaging at 7 T and beyond. *Eur Radiol Exp* 2021; 5: 35.
42. Tian Q, Wintermark M, Jeffrey Elias W, et al. Diffusion MRI tractography for improved transcranial MRI-guided focused ultrasound thalamotomy targeting for essential tremor. *Neuroimage Clin* 2018; 19: 572–580.